# EMG-based Hybrid Impedance-Force Control for Human-Robot Collaboration on Ultrasound Imaging*

Teng Li[1], Hongjun Xing[2], Hamid D. Taghirad[1,3], and Mahdi Tavakoli[1], *Senior Member, IEEE*

*Abstract*— Ultrasound (US) imaging is a common but physically demanding task in the medical field, and sonographers may need to put in considerable physical effort for producing high-quality US images. During physical human-robot interaction on US imaging, robot compliance is a critical feature that can ensure human user safety while automatic force regulation ability can help to improve task performance. However, higher robot compliance may mean lower force regulation accuracy, and vice versa. Especially, the contact/non-contact status transition can largely affect the control system stability. In this paper, a novel electromyography (EMG)-based hybrid impedance-force control system is developed for US imaging task. The proposed control system incorporates the robot compliance and force regulation ability via a hybrid controller while the EMG channel enables the user to online modulate the trade-off between the two features as necessary. Two experiments are conducted to examine the hybrid controller and show the necessity of involving an EMG-based modulator. A proof-of-concept study on US imaging is performed with implementing the proposed EMG-based control system, and the effectiveness is demonstrated. The proposed control system is promising to ensure robot's stability and patient's safety, thus obtain high-quality US images, while monitoring and reducing sonographer's fatigue. Furthermore, it can be easily adapted to other physically demanding tasks in the field of medicine.

## I. INTRODUCTION

During human-human collaboration, *e.g.*, lifting and moving a heavy box together, one naturally assumes to be the leader, while the other be the follower [1]. Aiming for good performance on a collaborated task, the follower is required to be able to shift between "compliant" and "rigid" behaviors whenever necessary according to the leader's intention. This is also true for human-robot collaboration when the human is the leader, in which case the robot is expected to be able to understand the user's intention and adapt its compliance level in real-time according to the requirement of the task.

[1]T. Li, H. D. Taghirad, and M. Tavakoli are with the Department of Electrical and Computer Engineering, Faculty of Engineering, University of Alberta, Edmonton T6G 1H9, Alberta, Canada. E-mail: {teng4, h.taghirad, mahdi.tavakoli}@ualberta.ca

[2]H. Xing is with the College of Astronautics, Nanjing University of Aeronautics and Astronautics, Nanjing 210016, China. E-mail:xinghj@nuaa.edu.cn

[3]H. D. Taghirad is with the Advanced Robotics and Automated Systems (ARAS), Industrial Control Center of Excellence, Faculty of Electrical Engineering, K. N. Toosi University of Technology, Tehran, Iran. E-mail: taghirad@kntu.ac.ir
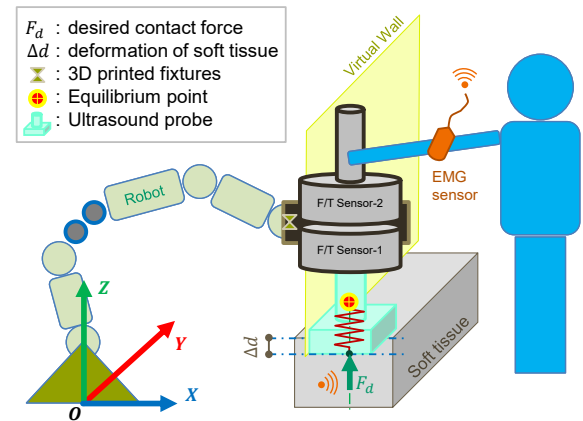
Fig. 1: Schematic setup of an EMG-based hybrid impedance-force control system for human-robot collaboration on Ultrasound imaging task.

Ultrasound (US) imaging task is conducted by sonographer in a way that manually holding and moving the US probe on patient's body or target tissue. This procedure demands considerable physical effort from the sonographer due to multitasking requirement, *e.g.*, regulating the probe-tissue contact force while moving the probe along a trajectory. Various robot-assisted US imaging methods [2] have been developed aiming both to reduce the sonographer's physical effort and to improve the task performance, *i.e.*, acquiring high-quality scanning images.

Robot teleoperation has been used for US imaging for a long time. Two decades ago, Mitsuishi *et al.* [3] developed a remote US diagnostic system. The distance between the user interface and teleoperated manipulator holding the US probe was about 700 km. Conti *et al.* [4] presented a new teleoperation robotic system assisting sonographers to conduct US imaging task aiming to reduce physical fatigue and better interpretation of US imaging data.

Apart from teleoperation systems, physical human-robot interaction (*p*HRI) for a collaborative US imaging task is very beneficial to sonographers. Carriere *et al.* [5] designed an admittance-controlled semi-autonomous system for US imaging. Their system enabled the robot to automatically control the US probe's orientation and the probe-tissue contact force, while the user controls the lateral position of the probe on the patient's body. In their system, 3D reconstruction technique is used to model the tissue surface.

To obtain compliant behavior from a robot, impedance/

admittance controller may be employed [1]. In *p*HRI applications, the robot can be controlled to be soft (compliant) or rigid (non-compliant) based on identified human intention and task requirements [6]. One main advantage of impedance control is its potentially better compliant robot behavior compared to admittance control. Another advantage is that the measurement or estimation on human-robot interaction force is not necessary for impedance control whereas it is indispensable for admittance control. On the other hand, implementing an impedance controller is usually more complex than an admittance controller because it usually requires full knowledge of the robot dynamics and accurately identified dynamic parameters [5].

Stable and appropriate normal contact force between the US probe and the tissue during scanning is one of the most important factors that can guarantee the US image quality [4], [5]. Different exam types may need different desired contact force range [7]. The requirement on accurately regulating the contact force into a desired range is a major reason that induces the sonographer's fatigue which could further affect image quality and even patient's safety. Force tracking controller allows a robot to track or regulate the robot-environment interaction force in an autonomous manner, which could effectively help the sonographer to do the force regulation during scanning [5].

Electromyography (EMG) is increasingly incorporated into robot control systems for better interpreting human intention and enhancing *p*HRI, because it can be more easily measured than some other physiological signals like electroencephalography (EEG) and electrocardiography (ECG). The concept of teleimpedance was first introduced in a work done by Ajoudani *et al.* [8], where the EMG measured from the human arm was used to regulate the robot impedance in real-time. By using EMG signal, the robot impedance was modified as needed in different phases of a *p*HRI task like peg-in-hole insertion. EMG was also used for online monitoring the user's fatigue during a *p*HRI task such that the robot could adapt itself to take over more physical work and allow the human partner to have some rest [9].

Contact/non-contact status switching is commonly encountered during US imaging especially at the start/end phase of the task. A critical issue during the status transition is that it can adversely affect the system stability thus patient's safety. Aiming to incorporate robot compliance and force regulation ability together while ensuring robot's stability especially during contact/non-contact status transition, in this paper, an EMG-based hybrid impedance-force control system is developed as shown in Fig. 1. The proposed system incorporates advantages of compliant robot behavior coming from an impedance controller and accurate force regulation ability coming from a force controller, while the EMG signal is used as a modulator which enables the human user to tune the trade-off between robot compliance and force regulation ability in an online manner. The effectiveness of the proposed control system is evaluated by a preliminary application on human-robot collaborated US imaging task.

The remainder of this paper is organized as follows: Section II describes the methods in detail including impedance control, force control, EMG signal processing and mapping. Section III presents the experiments and corresponding results for developing and evaluating the proposed control system, and concluding remarks are given in section IV.

## II. METHODS

### A. Impedance control and force control

The general dynamic model for an $n$-degree-of-freedom (DOF) rigid robot [10] may be expressed as

$$\mathbf{M}(\mathbf{q})\ddot{\mathbf{q}} + \mathbf{S}(\mathbf{q},\dot{\mathbf{q}})\dot{\mathbf{q}} + \mathbf{g}(\mathbf{q}) = \tau + \mathbf{J^T}\mathbf{F_{ext}} \qquad (1)$$

where $\mathbf{M} \in \mathbb{R}^{n \times n}$ denotes the inertia matrix, $\mathbf{S} \in \mathbb{R}^{n \times n}$ denotes a matrix related to the Coriolis and centrifugal forces, $\mathbf{g} \in \mathbb{R}^n$ represents a vector related to gravity, $\tau \in \mathbb{R}^n$ is the commanded joint torque vector, $\mathbf{F_{ext}} \in \mathbb{R}^6$ is external force in Cartesian space, and $\mathbf{J} \in \mathbb{R}^{6 \times n}$ is the Jacobian matrix. A full impedance model [11] can be expressed as

$$\mathbf{F_{imp}} = \mathbf{M_m}(\ddot{\mathbf{x}} - \ddot{\mathbf{x}_d}) + \mathbf{D_m}(\dot{\mathbf{x}} - \dot{\mathbf{x}_d}) + \mathbf{K_m}(\mathbf{x} - \mathbf{x_d})$$
$$(2)$$

where $\mathbf{M_m}, \mathbf{D_m}, \mathbf{K_m}$ are the user-defined matrices for inertia, damping, and stiffness, respectively. $\mathbf{x_d}, \dot{\mathbf{x}_d}, \ddot{\mathbf{x}_d}$ are the desired position, velocity, and acceleration, respectively in Cartesian space, while $\mathbf{x}, \dot{\mathbf{x}}, \ddot{\mathbf{x}}$ are the actual position, velocity, and acceleration, respectively. $\mathbf{F_{imp}} \in \mathbb{R}^6$ is the contact wrench (force and torque) between the robot end-effector (EE) and the environment in Cartesian space.

To avoid external force measurement, we set the desired inertia matrix equal to the natural inertia matrix of the robot, *i.e.*, $\mathbf{M_m} = \mathbf{M_x}$, where $\mathbf{M_x}$ is the natural inertia of the robot in Cartesian space, and $\mathbf{M_x} = \mathbf{J^{-T}MJ^{-1}}$ [12]. In order to represent a real mechanical system, a Coriolis and centrifugal term should also be included into the impedance model (2). Then, the full impedance model is augmented as

$$\mathbf{F_{imp}} = \mathbf{M_x}(\ddot{\mathbf{x}} - \ddot{\mathbf{x}_d})$$
$$+ (\mathbf{S_x} + \mathbf{D_m})(\dot{\mathbf{x}} - \dot{\mathbf{x}_d}) + \mathbf{K_m}(\mathbf{x} - \mathbf{x_d}) \qquad (3)$$

where $\mathbf{S_x}$ is the Coriolis and centrifugal matrix of the robot in Cartesian space and $\mathbf{S_x} = \mathbf{J^{-T}SJ^{-1}} - \mathbf{M_x}\dot{\mathbf{J}}\mathbf{J^{-1}}$. For set-point regulation problem, it has $\ddot{\mathbf{x}_d} = \dot{\mathbf{x}_d} = \mathbf{0}$. Then by substituting (3) into (1) via $\mathbf{F_{ext}} = \mathbf{F_{imp}}$, a simplified impedance control law can be obtained as given by (4), which is also known as task-space PD controller with gravity compensation.

$$\tau_{\mathbf{imp}} = \mathbf{J^T}[\mathbf{K_m}(\mathbf{x_d} - \mathbf{x}) - \mathbf{D_m}\dot{\mathbf{x}}] + \mathbf{g}, \qquad (4)$$

A general form of Cartesian-space force tracking controller [13] can be expressed as

$$\tau_{\mathbf{f}} = \mathbf{K_p}\mathbf{J^T}(\mathbf{F} - \mathbf{F_d})$$
$$+ \mathbf{K_i}\mathbf{J^T} \int_{\mathbf{0}}^{\mathbf{t}} (\mathbf{F} - \mathbf{F_d})\mathbf{dt} + \mathbf{K_d}\mathbf{J^T}(\dot{\mathbf{F}} - \dot{\mathbf{F}_d}) \qquad (5)$$

where $\mathbf{K_p}, \mathbf{K_i}, \mathbf{K_d} \in \mathbb{R}^{n \times n}$ are the gain matrices of P-regulator, I-regulator, and D-regulator, respectively in the joint space, which need to be designed. $\mathbf{F_d}, \mathbf{F} \in \mathbb{R}^6$ are the
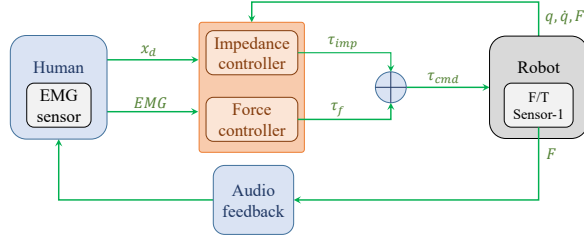
Fig. 2: Block diagram for the proposed EMG-based hybrid impedance-force control system.

desired and actual interaction force between the robot EE and the environment, respectively. For simplicity, a simplified PI force tracking controller is employed which is given by

$$\tau_{\mathbf{f}} = \mathbf{K_p}\mathbf{J^T}(\mathbf{F} - \mathbf{F_d}) + \mathbf{K_i}\mathbf{J^T} \int_{\mathbf{0}}^{\mathbf{t}} (\mathbf{F} - \mathbf{F_d})\mathbf{dt} \quad (6)$$

where $\mathbf{F}$ is measured by an external Force/Torque (F/T) sensor, $\mathbf{K_p} = k_p\mathbf{I}$, $\mathbf{K_i} = k_i\mathbf{I}$, and $\mathbf{I}$ is an appropriate identity matrix. Theoretically, the P-regulator ($\mathbf{K_p}$) term can be viewed as a spring which reduces the force error between $\mathbf{F}$ and $\mathbf{F_d}$. The I-regulator ($\mathbf{K_i}$) term acts as a compensator which can compensate the possible steady state force error.

The block diagram of the proposed EMG-based hybrid impedance-force control system for human-robot collaboration task is shown in Fig. 2. EMG-related processing and mapping methods will be introduced subsequently.

### B. EMG signal acquisition and processing

In this paper, raw electromyography (EMG) signal from human user's arm (biceps brachii) [14] is collected and processed in real-time. A simple moving average (SMA) algorithm given by (7) is employed as the filter.

$$e_{\mathtt{sma}} = \frac{1}{N} \sum_{n=1}^{N} e_{\mathtt{raw}} \quad (7)$$

where $e_{\mathtt{sma}}$ is the filtered EMG signal, $N$ is the moving window size in units of sample points, $e_{\mathtt{raw}}$ is the raw EMG.

After passing through a filter, the filtered EMG signal $e_{\mathtt{sma}}$ is normalized into a range of $[0, 1]$ by $e_{\mathtt{norm}} = e_{\mathtt{sma}}/e_{\mathtt{mvc}}$, via a user-specific parameter called maximum voluntary contraction (MVC). Therefore, the MVC needs to be calibrated for each user. The calibration procedure [14] is that, the user maximize his/her arm muscle effort for three times, then the average of the three maximum, denoted by $e_{\mathtt{mvc}}$, will be taken as the MVC of this user.

### C. EMG mapping algorithm

The normalized EMG signal $e_{\mathtt{norm}}$ is mapped to the P-regulator ($\mathbf{K_p} = k_p\mathbf{I}$ in (6)) in the hybrid impedance-force controller using the following mapping algorithm,

$$k_p = \begin{cases} (k_{p,max} - k_{p,min}) \times (1 - e_{\mathtt{norm}}) & \text{if } e_{\mathtt{norm}} \le \sigma \\ k_{p,min} & \text{if } e_{\mathtt{norm}} > \sigma \end{cases} \quad (8)$$

where $0 < \sigma < 1$, $k_{p,min}$ and $k_{p,max}$ represent the minimum and maximum force regulation ability of the robot,

respectively. The transition between the two conditions in (8) is realized via a low-pass filter to ensure the smoothness.

The general idea of the mapping algorithm (8) is that, when the human user exerts a larger interaction force on the robot EE (detected by Sensor 2 in Fig. 1), the robot should become more compliant. When the user exert a large-enough force ($e_{\mathtt{norm}} > \sigma$) on the robot EE, it indicates that the user intends to totally control the robot, thus the robot should provide the maximum compliance ($k_p = k_{p,min}$). To the contrary, when the user relaxes his/her arm ($e_{\mathtt{norm}} \le \sigma$), the robot should assume control of the contact force between the probe and tissue for an accurate force regulation, such that the user can focus on other tasks.

### D. Desired force and audio feedback design

As introduced in the Introduction, different purposes may require different desired force range for the contact force between the US probe and the tissue. Empirically, a desired range of $4.5 \pm 1$ N for the contact force is used in this paper for pilot tests. Note that in the force controller, it is possible to set other constant or time-varying desired force.

Accordingly, audio feedback is provided to the user to indicate which range the current normal contact force is located in, *i.e.*, lower range $[-inf, 3.5]$ N, ideal range $[3.5, 5.5]$ N, or upper range $[5.5, inf]$ N. Continuous beep is provided via Arduino board to indicate the ideal range, while discontinuous fast beep is provided to indicate the upper range. Otherwise, no audio feedback is provided.

## III. EXPERIMENTS AND RESULTS

### A. Apparatus

A 7-DOF Franka Emika Panda robot (Franka Emika GmbH, Munich, Germany) is employed for developing and evaluating the proposed EMG-based hybrid impedance-force control system for US imaging task as illustrated in Fig. 1. The hybrid controller is implemented via `libfranka`, the C++ implementation of the client side of the Franka Control Interface (FCI). The `libfranka` run with ROS control on a workstation computer of Intel(R) Core(TM) i5-8400 CPU @ 2.80GHz $\times$ 6 with the Ubuntu 16.04 LTS (Xenial Xerus) 64-bit operating system. The control rate of the robot is 1 kHz.

A classical Arduino MEGA2560 (R3) board is used to collect the raw EMG signal from EMG sensor and then transmit it to the control system. Meanwhile, it also provides audio feedback to the user to indicate the real-time contact status between the US probe and the soft tissue. The EMG signal sent from Arduino to the robot controller is at 1 kHz.

In this paper, the contact force between the US probe and the soft tissue is measured by a 6-DOF F/T sensor (Sensor 1 in Fig. 1, Axia80-M20-ZC22, ATI Industrial Automation, Inc., USA). Meanwhile, a second F/T sensor (Sensor 2 in Fig. 1) with exactly the same type is used to measure the external interaction force exerted by the human as an independent measurement to indicate the user effort. Please note that the data from Sensor 2 is only used for post-analysis and not used in the control system, and Sensor 2 can be removed in the future in order for a more compact system.

TABLE I: Parameters for the experiments.

| Parameter | Equation | Experiment |
|---|---|---|
| $\mathbf{K_m} = diag\{10, 10, 10, 0, 0, 0\}$ | (4) | Exp.1,2,3 |
| $\mathbf{D_m} = diag\{0, 0, 0, 0, 0, 0\}$ | (4) | Exp.1,2,3 |
| $\mathbf{F_d} = [0, 0, 4.5, 0, 0, 0]^T$ | (6) | Exp.1,2,3 |
| $k_p = 3$; $k_i = 0.5$ | (6) | Exp.1,3 |
| $k_p = 0/1/3$; $k_i = 0.5$ | (6) | Exp.2 |
| $k_{p,min} = 0$; $k_{p,max} = 3$; $\sigma = 0.5$ | (8) | Exp.2,3 |

Note: $\mathbf{K_m}, \mathbf{D_m} \in \mathbb{R}^{6 \times 6}$ are diagonal matrices. The desired contact force $\mathbf{F_d}$ is defined in the frame of Sensor 1, then transformed into the robot base frame. A preliminary test on $k_i$ at three levels ($k_i = 0/0.2/0.5$) was conducted, then $k_i = 0.5$ was determined based on the optimal results. $\sigma = 0.5$ is determined for a balanced level of human user's arm muscle contraction.

The main parameters used in the experiments are listed in Table I. The experiments are shown in the attached video[1].

### B. Experiment 1: Hybrid impedance-force controller

Experiment 1 is designed to evaluate the hybrid impedance-force controller in two scenarios. The first scenario is US imaging on a rectangular soft tissue as shown in Fig. 3a, and the second scenario is on bowl-shaped soft tissue (representing human breast) as shown in Fig. 3c.

A user performs an US imaging task in the two scenarios separately. In each trial, the user moves the US probe on the surface of the soft tissue from one side to the other and then back. Three continuous trials compose as one session, and six sessions for each scenario. Note that, this experiment does not involve contact/non-contact status transition.

A typical sample data for each of the two scenarios are shown in Fig. 3b and Fig. 3d. The detailed results of Experiment 1 are summarized in Table II. These results show that the performance in rectangular scenario has no significant difference ($p = 0.2542$) with that in bowl-shaped scenario in terms of normal force regulation accuracy. However, the rectangular scenario has significantly more stable force regulation behavior ($p = 0.0097$) than the bowl-shaped scenario in terms of standard deviation. This is reasonable considering that the latter scenario involves more complex rotational movements while the former does not.

The results of Experiment 1 indicate that, the hybrid impedance-force controller is able to help the user regulate the probe-tissue contact force in both simple (rectangular) scenario and complex (bowl-shaped) scenario without significant difference in terms of average contact force. With the help of the hybrid controller, the robot will regulate the contact force while the user can focus on other tasks, *e.g.*, moving the probe on the tissue along a desired trajectory.

### C. Experiment 2: Lifting task

During US imaging, contact/non-contact status transition, *e.g.*, moving the probe away from or onto the tissue surface, is a major factor that could affect the control system stability,

[1]online video link: https://drive.google.com/file/d/11l-Xsanpz_Wuui8YEb0hoxj_SUAqwiBm/view?usp=sharing



(a) Rectangular scenario



(b) Sample data (rect.)



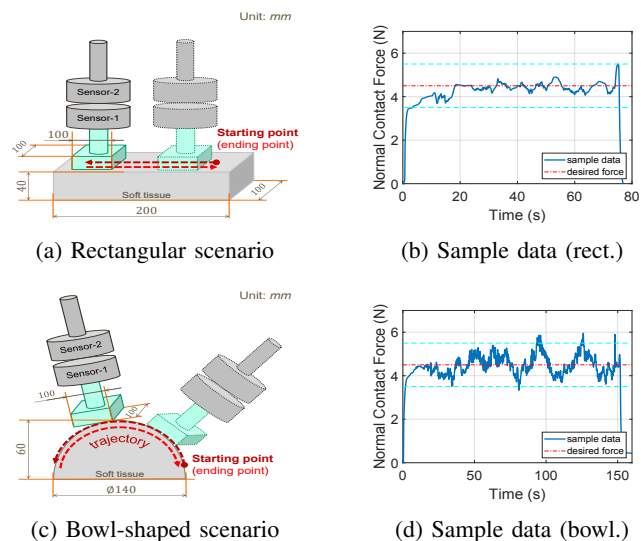(c) Bowl-shaped scenario



(d) Sample data (bowl.)

Fig. 3: Schematic illustration for the two scenarios in Experiment 1 and typical sample results. Two cyan dash lines indicate the predefined ideal range $[3.5, 5.5]$ N, while the red dash-dot line denotes the desired force $4.5$ N.

TABLE II: Results of Experiment 1 on normal contact force in rectangular and bowl-shaped tissue scenarios.

| | Mean (N) | | std. (N) | |
|---|---|---|---|---|
| | Rect. | Bowl. | Rect. | Bowl. |
| s1 | 4.426 | 4.517 | 0.291 | 0.461 |
| s2 | 4.446 | 4.397 | 0.245 | 0.581 |
| s3 | 4.390 | 4.473 | 0.249 | 0.359 |
| s4 | 4.304 | 4.431 | 0.369 | 0.458 |
| s5 | 4.438 | 4.456 | 0.167 | 0.543 |
| s6 | 4.472 | 4.432 | 0.293 | 0.430 |
| | $p = 0.2542$ | | $p = 0.0097$ (*) | |

Note: s1, means session-1; Rect., means rectangular tissue scenario; Bowl., means bowl-shaped tissue scenario; std., means standard deviation.

thus potentially endanger the patient's safety. Therefore, it is necessary to examine the system stability and robot compliance when contact/non-contact status transition is involved. For this purpose, a lifting task is designed in Experiment 2 as illustrated in Fig. 4a. In each trial, the user needs to lift the US probe from one surface to a predefined height and then move onto another surface. During the task, the maximum force exerted by the user is measured by the F/T Sensor 2 and recorded as the user's effort in each trial. There are three levels for the P-regulator are tested due to a mapping relationship between the EMG signal and the P-regulator in the final controller. Six trials for each level are conducted.

The results on the lifting task are shown in Fig. 4b. As can be seen in the figure, the user's maximum efforts significantly increase as the increasing of the P-regulator. This means that with a lower level of $k_p$, the robot can provide better compliance, thus the user can easily lift and move the US probe. However, with a higher level of $k_p$, the robot can
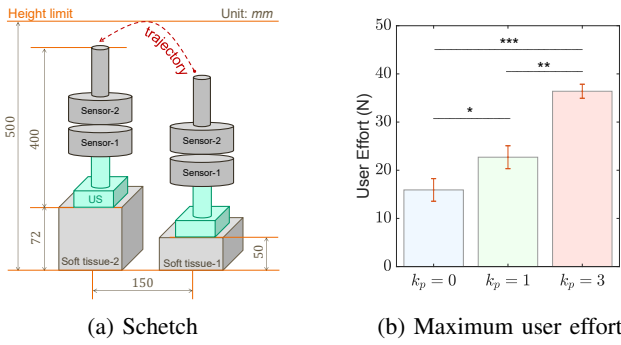
(a) Schetch  (b) Maximum user effort

Fig. 4: Schematic illustration and results for the lifting task in Experiment 2. The maximum user effort are from three levels of the P-regulator in the PI force controller.



Fig. 5: Setup for the application in Experiment 3 with implementing the EMG-based hybrid impedance-force controller.

provide better force regulation accuracy but the user needs to make more effort to lift the US probe. More importantly, the latter case could easily trigger an unstable system due to the potentially large external force, *e.g.*, trigger an automatic emergency stop for the Panda robot.

The results of Experiment 2 indicate that, the P-regulator in the force controller is able to do a trade-off between the robot compliance and the force regulation ability. An EMG-based modulator will be introduced into the control system such that the trade-off can be tuned online by the user.

### D. Experiment 3: Application

In Experiment 3, a proof-of-concept application study on the US imaging is conducted by implementing the proposed EMG-based hybrid impedance-force controller. The user's arm EMG signal is mapped with the P-regulator of the force controller via the algorithm (8). This allows not only the robot to regulate the contact force autonomously, but also the user to modulate the robot compliance in an online manner.

As shown in Fig. 5, a general US imaging task is designed in Experiment 3 to evaluate the effectiveness of the proposed EMG-based hybrid controller. The task includes a lifting sub-task that involves contact/non-contact status transition, and an US imaging sub-task on a complex tissue surface geometry which consists of a horizontal plane and an inclined slope plane. For each trial in the task, the user first needs to lift the US probe to reach a predefined height (the same height as that in Experiment 2), then puts it onto the complex tissue surface, and then moves it on the surface to the end and then back (see the red dash trajectory in the figure). To assist the user in moving the probe along the trajectory, a vertical virtual wall is set along the trajectory. Six separate sessions are conducted and each session includes only one trial. The user effort, *i.e.*, maximum lifting force, and normal contact force are recorded in each session.

A sample data for a typical session in Experiment 3 is presented in Fig. 6. As shown in the figure, the first colored area is for the lifting sub-task that involves contact/non-contact status transition while the second colored area is for the US imaging sub-task. The area between the two colored areas is a recovery phase in which the contact force will
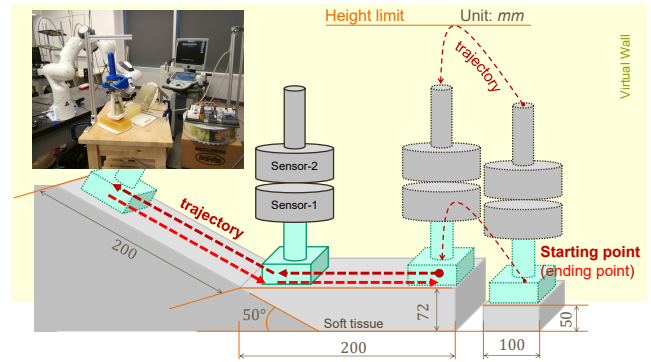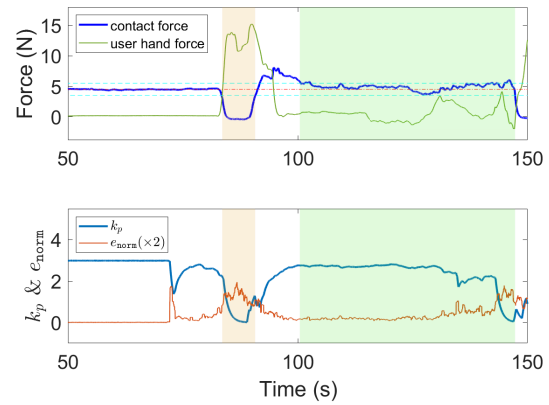


Fig. 6: Sample data for a typical trial in Experiment 3. The yellow colored area is for the lifting sub-task while the green colored area is for the US imaging sub-task.

recovered to the desired level driven by the hybrid controller. The maximum user effort in the lifting sub-task and the normal contact force in the US imaging sub-task in each session are summarized in Table III. As shown in the table and Fig. 6, with the help of EMG-based modulator, the robot compliance can be tuned online as needed, and the user effort for lifting the probe is kept in a reasonable range, which ensure system stability and patient's safety.

A comparison is conducted between the results of Experiment 3 and the two scenarios in Experiment 1 as show in Fig. 7. As can be seen in Fig. 7a, there is no significant difference in terms of the force regulation accuracy between the scenario in Experiment 3 and either of the rectangular and bowl-shaped tissue scenarios in Experiment 1. This indicates that the performance on force regulation accuracy in Experiment 3 is as good as that in the rectangular and bowl-shaped tissue scenario in Experiment 1. For the standard deviation as shown in Fig. 7b, however, there is significant difference ($p = 0.002$) between Experiment 3 and the rectangular scenario in Experiment 1 which indicates that the latter had a significantly more stable force regulation behavior. This is reasonable since the latter scenario has not involved complex

TABLE III: Results of Experiment 3 with the proposed EMG-based hybrid impedance-force controller.

| | Normal contact force (N) | | User effort (N) |
| | mean | std. | max |
| --- | --- | --- | --- |
| s1 | 4.848 | 0.663 | 16.319 |
| s2 | 4.881 | 0.479 | 15.241 |
| s3 | 4.615 | 0.764 | 14.807 |
| s4 | 4.554 | 0.575 | 16.021 |
| s5 | 4.379 | 0.725 | 16.092 |
| s6 | 4.424 | 0.898 | 16.502 |

Note: s1, means session-1; std., means standard deviation.
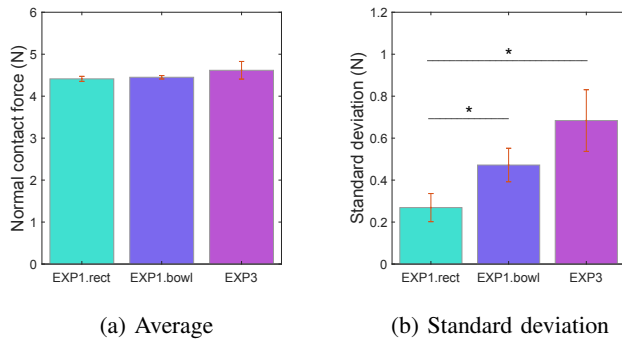


(a) Average      (b) Standard deviation

Fig. 7: Comparison between Experiment 3 and the two scenarios (rectangular and bowl-shaped) in Experiment 1. Note, EXP1.rect and EXP1.bowl mean rectangular scenario and bowl-shaped scenario in Experiment 1, respectively.

rotations of the robot EE. There is no significant difference on the standard deviation ($p = 0.053$) between Experiment 3 and the bowl-shaped scenario in Experiment 1.

One limitation of the proposed EMG-based method is that the EMG acquisition system needs to be calibrated for each individual in order to obtain the MVC, although the calibration procedure is simple. In the future work, machine learning algorithms will be employed to automatically identify the MVC online and on a user-specific basis. Another limitation is that normal contact force rather than acquired image is used as the metric to evaluate the proposed system in the present work. Although the contact force is a main indicator for obtaining high-quality US scanning images, directly evaluating the quality of the acquired scanning images will be a necessary part for evaluating the effectiveness of the proposed system in future work. Also, user performance study on the proposed system needs to be systematically conducted and evaluated in the next step by medical experts like sonographers. The EMG acquisition device with wired connection is cumbersome to some extent for the operator in our current experiment. In future work, wireless communication will be employed for a more compact system.

## IV. CONCLUSIONS

Contact status transition between contact and non-contact is a main factor that may cause system instability. Compliant robot behavior can be expected from an impedance controller during physical human-robot interaction while accurate force regulation can be expected from a force controller. However, higher compliance may mean lower force regulation accuracy, and vice versa. In this paper, a novel EMG-based hybrid impedance-force control system for human-robot collaborative Ultrasound (US) imaging task is developed and evaluated. The proposed control system incorporates the robot compliance and force regulation ability via a hybrid impedance-force controller. EMG signal of the user is mapped with the hybrid controller as a modulator which allows the user to tune the trade-off between robot compliance and force regulation ability in an online manner. The effectiveness of the proposed control system is demonstrated by a proof-of-concept application study on US imaging.

The proposed control system is promising to be used in the US imaging task for monitoring the sonographer's fatigue, ensuring the patient's safety, and improving US imaging quality. This proposed system can be easily adapted to many other medical tasks that require strenuous physical human effort like procedures in orthopedic surgery.

## REFERENCES

[1] D. P. Losey *et al.*, "A review of intent detection, arbitration, and communication aspects of shared control for physical human–robot interaction," *Applied Mechanics Reviews*, vol. 70, no. 1, 2018.

[2] A. M. Priester, S. Natarajan, and M. O. Culjat, "Robotic ultrasound systems in medicine," *IEEE transactions on ultrasonics, ferroelectrics, and frequency control*, vol. 60, no. 3, pp. 507–523, 2013.

[3] M. Mitsuishi *et al.*, "Remote ultrasound diagnostic system," in *2001 IEEE International Conference on Robotics and Automation (ICRA)*, vol. 2. IEEE, 2001, pp. 1567–1574.

[4] F. Conti, J. Park, and O. Khatib, "Interface design and control strategies for a robot assisted ultrasonic examination system," in *Experimental Robotics*. Springer, 2014, pp. 97–113.

[5] J. Carriere *et al.*, "An admittance-controlled robotic assistant for semi-autonomous breast ultrasound scanning," in *2019 international symposium on medical robotics (ISMR)*. IEEE, 2019, pp. 1–7.

[6] M. Li and A. M. Okamura, "Recognition of operator motions for real-time assistance using virtual fixtures," in *11th Symposium on Haptic Interfaces for Virtual Environment and Teleoperator Systems, 2003. HAPTICS 2003. Proceedings.* IEEE, 2003, pp. 125–131.

[7] N. Smith-Guerin *et al.*, "Clinical validation of a mobile patient-expert tele-echography system using isdn lines," in *4th International IEEE EMBS Special Topic Conference on Information Technology Applications in Biomedicine, 2003.* IEEE, 2003, pp. 23–26.

[8] A. Ajoudani, N. Tsagarakis, and A. Bicchi, "Tele-impedance: Teleoperation with impedance regulation using a body–machine interface," *The International Journal of Robotics Research*, vol. 31, no. 13, pp. 1642–1656, 2012.

[9] L. Peternel *et al.*, "Robot adaptation to human physical fatigue in human–robot co-manipulation," *Autonomous Robots*, vol. 42, no. 5, pp. 1011–1021, 2018.

[10] J. Fong, H. Rouhani, and M. Tavakoli, "A therapist-taught robotic system for assistance during gait therapy targeting foot drop," *IEEE Robotics and Automation Letters*, vol. 4, no. 2, pp. 407–413, 2019.

[11] H. Xing *et al.*, "An admittance-controlled wheeled mobile manipulator for mobility assistance: Human–robot interaction estimation and redundancy resolution for enhanced force exertion ability," *Mechatronics*, vol. 74, p. 102497, 2021.

[12] A. Torabi *et al.*, "Application of a redundant haptic interface in enhancing soft-tissue stiffness discrimination," *IEEE Robotics and Automation Letters*, vol. 4, no. 2, pp. 1037–1044, 2019.

[13] C. Schindlbeck and S. Haddadin, "Unified passivity-based cartesian force/impedance control for rigid and flexible joint robots via task-energy tanks," in *2015 IEEE International Conference on Robotics and Automation (ICRA)*. IEEE, 2015, pp. 440–447.

[14] P. Konrad, "The abc of EMG," *A practical introduction to kinesiological electromyography*, vol. 1, no. 2005, pp. 30–5, 2005.